AD-A117 622 PENNSYLVANIA STATE UNIV UNIVERSITY PARK APPLIED RESE--ETC F/G 20/11
ELASTIC/PLASTIC FINITE ELEMENT ANALYSIS OF A SINGLE EDGE-CRACKE--ETC(U)
MAY 82 E P MOSKAL N00024-79-C-6043
UNCLASSIFIED ARL/PSU/TR-82-131 NL

END
DATE
FILMED
8 82
DTIC

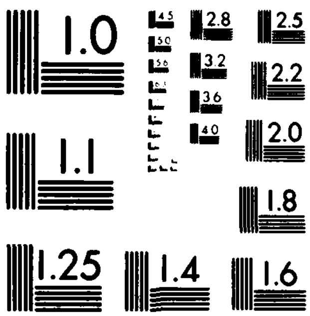

MICROCOPY RESOLUTION TEST CHART
NATIONAL BUREAU OF STANDARDS-1963-A

(6)

AD A117622

ELASTIC/PLASTIC FINITE ELEMENT ANALYSIS OF A SINGLE EDGE-CRACKED BEAM SUBJECTED TO MODE I TENSILE LOADING

Edward Paul Moskal

Technical Memorandum
File No. TM 82-131
May 24, 1982
Contract No. N00024-79-C-6043

Copy No. 5

The Pennsylvania State University
Intercollege Research Programs and Facilities
APPLIED RESEARCH LABORATORY
Post Office Box 30
State College, PA 16801

NAVY DEPARTMENT

NAVAL SEA SYSTEMS COMMAND

UNCLASSIFIED

SECURITY CLASSIFICATION OF THIS PAGE (When Data Entered)

REPORT DOCUMENTATION PAGE		READ INSTRUCTIONS BEFORE COMPLETING FORM
1. REPORT NUMBER 82-131	2. GOVT ACCESSION NO. AD-A117622	3. RECIPIENT'S CATALOG NUMBER
4. TITLE (and Subtitle) ELASTIC/PLASTIC FINITE ELEMENT ALALYSIS OF A SINGLE EDGE-CRACKED BEAM SUBJECTED TO MODE I TENSILE LOADING		5. TYPE OF REPORT & PERIOD COVERED M.S., Thesis, August 1982
		6. PERFORMING ORG. REPORT NUMBER 82-131
7. AUTHOR(s) Edward Paul MOSKAL		8. CONTRACT OR GRANT NUMBER(s) N00024-79-C-6043
9. PERFORMING ORGANIZATION NAME AND ADDRESS The Pennsylvania State University Applied Research Laboratory, P.O. Box 30 State College, PA 16801		10. PROGRAM ELEMENT, PROJECT, TASK AREA & WORK UNIT NUMBERS
11. CONTROLLING OFFICE NAME AND ADDRESS Naval Sea Systems Command Department of the Navy Washington, DC 20362		12. REPORT DATE May 24, 1982
		13. NUMBER OF PAGES 46 pages & figures
14. MONITORING AGENCY NAME & ADDRESS(if different from Controlling Office)		15. SECURITY CLASS. (of this report) Unclassified, Unlimited
		15a. DECLASSIFICATION/DOWNGRADING SCHEDULE

16. DISTRIBUTION STATEMENT (of this Report)

Approved for public release, distribution unlimited, per NSSC (Naval Sea Systems Command), 7/7/82

17. DISTRIBUTION STATEMENT (of the abstract entered in Block 20, if different from Report)

18. SUPPLEMENTARY NOTES

19. KEY WORDS (Continue on reverse side if necessary and identify by block number)

thesis, edge, cracked, beam

20. ABSTRACT (Continue on reverse side if necessary and identify by block number)

A thorough analysis of the stresses, strains and displacements surrounding the crack tip of a single edge-cracked beam subjected to Mode I tensile loading was performed by constructing various two-dimensional finite element models. Of particular interest in the analysis was 1) determination of the Mode I stress intensity factor in the elastic models and 2) examination of the size and character of the plastic zone in the elastic-perfectly plastic models.

The finite element program used in the investigation was BOPACE-3D (The

DD FORM 1 JAN 73 1473 EDITION OF 1 NOV 65 IS OBSOLETE

UNCLASSIFIED

SECURITY CLASSIFICATION OF THIS PAGE (When Data Entered)

Boeing Plastic Analysis Capability for Engines). In order to model the singularity effects at the crack tip, special "crack tip elements" were utilized immediately surrounding the crack tip. Different crack tip elements were used for the elastic models and the elastic-perfectly plastic models. Both coarse and fine-grid meshes were evaluated in the analysis.

The finite element model results are compared to various other solutions. Results for the elastic models are compared to available empirical solutions while the elastic-perfectly plastic results are examined with regard to extent and character of the elastic-plastic region.

ABSTRACT

A thorough analysis of the stresses, strains and displacements surrounding the crack tip of a single edge-cracked beam subjected to Mode I tensile loading was performed by constructing various two-dimensional finite element models. Of particular interest in the analysis was 1) determination of the Mode I stress intensity factor in the elastic models and 2) examination of the size and character of the plastic zone in the elastic-perfectly plastic models.

The finite element program used in the investigation was BOPACE-3D (The Boeing Plastic Analysis Capability for Engines). In order to model the singularity effects at the crack tip, special "crack tip elements" were utilized immediately surrounding the crack tip. Different crack tip elements were used for the elastic models and the elastic-perfectly plastic models. Both coarse and fine-grid meshes were evaluated in the analysis.

The finite element model results are compared to various other solutions. Results for the elastic models are compared to available empirical solutions while the elastic-perfectly plastic results are examined with regard to extent and character of the elastic-plastic region.

TABLE OF CONTENTS

	Page
ABSTRACT	iii
LIST OF TABLES	v
LIST OF FIGURES	vi
LIST OF SYMBOLS	vii
ACKNOWLEDGEMENTS	viii
I. INTRODUCTION	1
1.1 General Introduction	1
1.2 Purpose of the Investigation	2
1.3 Scope of the Investigation	2
II. ELASTIC-PLASTIC FINITE ELEMENT MODELING	3
2.1 General Concepts	3
2.2 Elastic and Elastic-Perfectly Plastic Crack Tip Elements	5
2.3 BOPACE	12
III. ANALYSIS OF A SINGLE EDGE-CRACKED BEAM SUBJECTED TO MODE I TENSILE LOADING	13
3.1 Method of Approach	13
3.2 Finite Element Meshes	13
3.3 Elastic Results and Discussion	16
3.4 Elastic-Perfectly Plastic Results and Discussion	27
IV. SUMMARY AND CONCLUSION	33
V. RECOMMENDATIONS FOR FUTURE RESEARCH	34
BIBLIOGRAPHY	36
APPENDIX A: ELASTIC CRACK-TIP STRESS AND DISPLACEMENT FIELDS	38
APPENDIX B: SINGLE EDGE NOTCH TEST SPECIMEN	40
APPENDIX C: STRAIN ENERGY RELATIONS	42
APPENDIX D: ELASTIC FINITE ELEMENT MODEL RESULTS	43

LIST OF TABLES

Table		Page
D-1.	Model A Displacement Results (Plane Stress Assumption)	43
D-2.	Model A Displacement Results (Plane Strain Assumption)	44
D-3.	Model B Displacement Results (Plane Stress Assumption)	45
D-4.	Model B Displacement Results (Plane Strain Assumption)	46

LIST OF FIGURES

Figure		Page
1.	Element Geometry.	6
2.	Elastic Finite Element Model A.	14
3.	Elastic Finite Element Model B.	15
4.	Elastic-Perfectly Plastic Finite Element Model C.	17
5.	Magnification of Crack Tip Region in Elastic-Perfectly Plastic Finite Element Model C.	18
6.	Finite Element Model A Results (Plane Stress Assumption).	19
7.	Finite Element Model B Results (Plane Stress Assumption).	20
8.	Finite Element Model A Results (Plane Strain Assumption).	21
9.	Finite Element Model B Results (Plane Strain Assumption).	22
10.	Finite Element Model A Results (Plane Stress Assumption).	23
11.	Finite Element Model B Results (Plane Stress Assumption).	24
12.	Finite Element Model A Results (Plane Strain Assumption).	25
13.	Finite Element Model B Results (Plane Strain Assumption).	26
14.	Plane Stress Plastic Zone Observed in Elastic-Perfectly Plastic Finite Element Model C.	28
15.	Plane Strain Plastic Zone Observed in Elastic-Perfectly Plastic Finite Element Model C.	29
16.	Elastic/Plastic Results (Plane Stress Assumption)	30
17.	Elastic/Plastic Results (Plane Strain Assumption)	31
A1.	Mode I Loading.	39
B1.	Edge Notch Speciman	41

LIST OF SYMBOLS

σ_{ij}	normal and shear stress components
G_I	strain energy release rate
ν	Poisson's ratio
E	Young's modulus of elasticity
G	shear modulus
ε_{ij}	strain tensor components
K_I	stress intensity factor for Mode I
r,θ,z	polar coordinates with origin at crack tip
x,y,z	cartesian coordinates
a	edge-crack length
u	displacement in x-direction
v	displacement in y-direction
b	width of model
ξ,η	coordinates of transformed system
N_i	shape functions
$[J]$	Jacobian matrix
$[D]$	stress-strain matrix
$[K]$	stiffness matrix

ACKNOWLEDGEMENTS

The author wishes to express his sincere appreciation to Dr. Joseph C. Conway, Associate Professor of Engineering Mechanics, for his sincere interest in providing assistance and encouragement in the research and preparation of this thesis. Appreciation is also extended toward Dr. Ganta B. Reddy, of Combustion Engineering, Inc., and Dr. Richard A. Queeney, Associate Professor of Engineering Mechanics, for their helpful advice.

The author would also like to thank the people in the Applied Research Laboratory for the financial support of the research along with those who have critiqued this thesis.

CHAPTER I

INTRODUCTION

1.1 General Introduction

Elastic and elastic-plastic fracture mechanics problems have received considerable interest for the past 20 years. A great deal of work in elastic fracture mechanics has been centered around the development of empirical solutions [14, 16], experimental techniques [17] and numerical methods [11] for the determination of Mode I stress intensity factors. Photoelasticity is one of the experimental techniques which has been used to predict stress intensity factors while finite element modeling is a numerical method which made its debut in this area of fracture mechanics in the early 1970's [11].

With the development of special "crack-tip elements," [2, 5, 7], finite element models currently represent the crack-tip singularity effects with a higher degree of accuracy. Not only do the finite element models better represent the singularity effects, but the models are able to do so with coarser meshes, which result in great savings in time and money.

In addition to the development of elastic crack-tip elements, finite element programs and crack-tip elements which represent plastic behavior have also been developed [6]. This has enabled the finite element modeling of elastic-perfectly plastic behavior. Specifically, plastic zone effects at the crack-tip can be modeled for various loading conditions and the size and character of the plastic zone may be exam'ned.

1.2 Purpose of the Investigation

The purpose of this investigation was to examine and evaluate recently developed, improved finite element techniques which can be applied to fracture mechanics problems. Particular emphasis was placed on evaluating both the elastic and elastic-perfectly plastic crack-tip elements in modeling a single edge-cracked beam subjected to Mode I tensile loading.

1.3 Scope of the Investigation

This investigation can be divided into four primary parts. The first part consists of generally analyzing the stress, strain and displacement distributions surrounding the crack-tip for a single edge-cracked elastic beam subjected to Mode I tensile loading. The second part consists of 1) determining elastic Mode I stress intensity factors using the displacements obtained from the elastic finite element model then 2) comparing the Mode I stress intensity factors determined from the finite element model to stress intensity factors resulting from a boundary collocation solution [16]. The third part of the investigation consists of generally analyzing the stress, strain and displacement distributions surrounding the crack-tip for a single edge-cracked elastic-perfectly plastic beam subjected to Mode I tensile loading. Finally, the fourth part consists of examining the size and character of the plastic zone surrounding the crack-tip for a single edge-cracked elastic-perfectly plastic beam subjected to Mode I tensile loading.

CHAPTER II

ELASTIC-PLASTIC FINITE ELEMENT MODELING

2.1 General Concepts

General concepts for the solution of elastic or elastic-plastic problems by means of isoparametric finite elements may be found in various references [5, 6, 15]. Using the notation found in Reference 6, the geometry of an 8-node plane isoparametric element is mapped into a normalized square space (ξ, η), through the following transformations,

$$x = \sum_{i=1}^{8} N_i(\xi, \eta)x_i$$

and (1)

$$y = \sum_{i=1}^{8} N_i(\xi, \eta)y_i,$$

where

$$N_i = \left[(1+ \xi\xi_i)(1 + \eta\eta_i)-(1-\xi^2)(1 + \eta\eta_i)-(1-\eta^2)(1 + \xi\xi_i)\right]\xi_i^2\eta_i^2/4$$
$$+ (1-\xi^2)(1 + \eta\eta_i)(1-\xi_i^2)\eta_i^2 /2 + (1-\eta^2)(1 + \xi\xi_i)(1-\eta_i^2)\xi_i^2 /2, \tag{2}$$

N_i = the shape function corresponding to node i, whose coordinates are (x_i, y_i) in the x-y system and (ξ_i, η_i) in the transformed ξ-η system

and

ξ_i, η_i = ± 1 for corner nodes
$\quad\quad$ 0 for mid-side nodes.

The displacements are interpolated by the same shape functions as

$$u = \sum_{i=1}^{8} N_i(\xi, \eta) u_i$$

and

$$v = \sum_{i=1}^{8} N_i(\xi, \eta) v_i . \tag{3}$$

The stiffness matrix is found through the following relationships,

$$\begin{bmatrix}\varepsilon\end{bmatrix} = \begin{bmatrix}B\end{bmatrix} \begin{bmatrix} u_i \\ v_i \end{bmatrix} \tag{4}$$

and
$$\begin{bmatrix}B\end{bmatrix} = \begin{bmatrix} \frac{\partial N_i}{\partial x} & 0 \\ 0 & \frac{\partial N_i}{\partial y} \\ \frac{\partial N_i}{\partial y} & \frac{\partial N_i}{\partial x} \end{bmatrix}, \tag{5}$$

where

$$\begin{bmatrix} \frac{\partial N_i}{\partial x} \\ \frac{\partial N_i}{\partial y} \end{bmatrix} = \begin{bmatrix}J\end{bmatrix}^{-1} \begin{bmatrix} \frac{\partial N_i}{\partial \xi} \\ \frac{\partial N_i}{\partial \eta} \end{bmatrix} \tag{6}$$

and the Jacobian matrix $\begin{bmatrix}J\end{bmatrix}$ is given by

$$\begin{bmatrix}J\end{bmatrix} = \begin{bmatrix} \frac{\partial x}{\partial \xi} & \frac{\partial y}{\partial \xi} \\ \frac{\partial x}{\partial \eta} & \frac{\partial y}{\partial \eta} \end{bmatrix} = \begin{bmatrix} \cdots\cdots \frac{\partial N_i}{\partial \xi} \cdots\cdots \\ \cdots\cdots \frac{\partial N_i}{\partial \eta} \cdots\cdots \end{bmatrix} \begin{bmatrix} \vdots & \vdots \\ x_i & y_i \\ \vdots & \vdots \end{bmatrix} . \tag{7}$$

The stress is given by

$$\left[\sigma\right] = \left[D\right] \left[\varepsilon\right] \tag{8}$$

where $\left[D\right]$ is the stress-strain matrix. The element stiffness matrix $\left[K\right]$ is then,

$$\left[K\right] = \int_{-1}^{1} \int_{-1}^{1} \left[B\right]^T \left[D\right] \left[B\right] \det|J| d\xi d\eta. \tag{9}$$

The above derivation considers the elastic case, however, a similar derivation at an incremental level can be performed for the plastic case.

In modeling fracture mechanics problems, a singularity must occur at the crack tip. Therefore, to obtain a singular element which will be used at the crack-tip, the stress and strain in equations (8) and (4) must be singular. The formation of crack-tip elements which model the crack-tip singularity is the topic of the following section.

2.2 Elastic and Elastic-Perfectly Plastic Crack-Tip Elements

One method used to create the singularity in the quadrilateral isoparametric elements, is to collapse an edge of the element and move the mid-side nodes to the quarter-points as shown in Figure 1. For the element shown in Figure 1, we have the following nodal coordinates,

$$x_1 = x_7 = x_8 = 0,$$

$$x_2 = x_6 = \frac{h}{4},$$

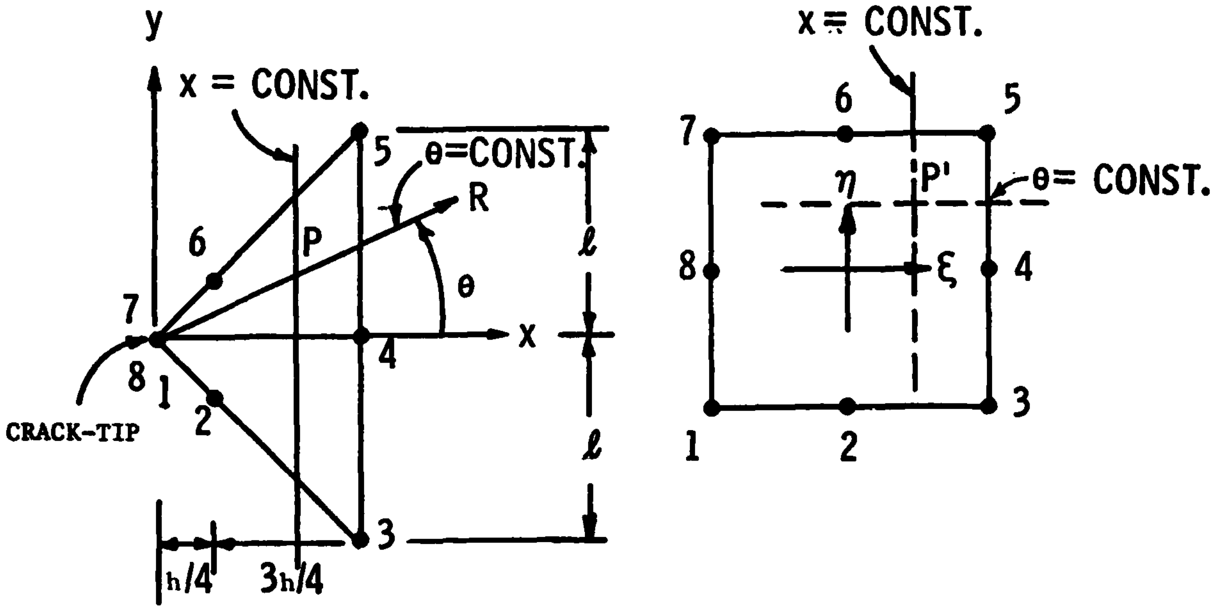

(a)

Two-dimensional crack-tip element

(b)

Parent element

Figure 1. Element Geometry.

$$x_3 = x_4 = x_5 = h,$$

$$y_1 = y_7 = y_8 = y_4 = 0, \tag{10}$$

$$y_2 = -y_6 = -\frac{\ell}{4}$$

and $y_3 = -y_5 = -\ell.$

Substituting the nodal conditions (10) in equations (1) and collecting terms yields

$$x = \frac{h}{4}(1+\xi)^2$$

and (11)

$$y = \frac{\ell}{4}\eta(1+\xi)^2.$$

Point P on the radial line R, is at a distanee r from the crack-tip, where $r = \sqrt{(x^2 + y^2)}$. Substituting from equations (11) yields

$$r = \frac{\ell}{4}(1+\xi)^2\sqrt{(\frac{h}{\ell})^2 + \eta^2}$$

where

$$(1+\xi) = \sqrt{r} \Bigg/ \sqrt{\frac{\ell}{4}\sqrt{(\frac{h}{\ell})^2 + \eta^2}}. \tag{12}$$

Substituting equations(11) in equation (7) yields

$$\left[J\right] = \begin{bmatrix} \frac{h}{2}(1+\xi) & \frac{\ell}{2}\,\eta(1+\xi) \\ 0 & \frac{\ell}{4}(1+\xi)^2 \end{bmatrix} \tag{13}$$

and its determinant

$$\det|J| = \frac{h\ell}{8}(1+\xi)^3. \tag{14}$$

Inverting,

$$\left[J\right]^{-1} = \begin{bmatrix} I_{11} & I_{12} \\ I_{21} & I_{22} \end{bmatrix} = \begin{bmatrix} \frac{2}{h(1+\xi)} & \frac{-4}{h(1+\xi)^2} \\ 0 & \frac{4}{\ell(1+\xi)^2} \end{bmatrix}. \tag{15}$$

Taking the derivatives of the displacements u and v with respect to ξ and η gives

$$\frac{\partial u}{\partial \xi} = \sum_{i=1}^{8} \frac{\partial N_i}{\partial \xi} u_i,$$

$$\frac{\partial u}{\partial \eta} = \sum_{i=1}^{8} \frac{\partial N_i}{\partial \eta} u_i, \tag{16}$$

$$\frac{\partial v}{\partial \xi} = \sum_{i=1}^{8} \frac{\partial N_I}{\partial \xi} v_i,$$

and

$$\frac{\partial v}{\partial \eta} = \sum_{i=1}^{8} \frac{\partial N_i}{\partial \eta} v_i.$$

Substituting for nodal numbers and performing the above operation will yield

$$\frac{\partial u}{\partial \xi} = \frac{u_1}{4}(-2+3\eta-\eta^2) + u_2(1-\eta) + \frac{u_3}{4}(\eta+\eta^2) + \frac{u_4}{2}(1-\eta^2)$$

$$-\frac{u_5}{4}(-\eta+\eta^2) + u_6(1+\eta) + \frac{u_7}{4}(-2-3\eta-\eta^2) - \frac{u_8}{2}(1-\eta^2) \tag{17}$$

$$+(1+\xi)\left[\frac{u_1}{2}(1-\eta) - u_2(1-\eta) + \frac{u_3}{2}(1-\eta) + \frac{u_5}{2}(1+\eta) - u_6(1+\eta) + \frac{u_7}{2}(1+\eta)\right]$$

and

$$\frac{\partial u}{\partial \eta} = \left[\frac{u_1}{4}(-2 + 4\eta) + \frac{u_7}{4}(2+4\eta) \; -2u_8\eta\right]^*$$

$$+ (1+\xi)\left[\frac{u_1}{4}(3-2\eta)-u_2 + \frac{u_3}{4}(1+2\eta) - u_4\eta + \frac{u_5}{4}(1-2\eta)+u_6 - \frac{u_7}{4}(-3+2\eta)+u_8\eta\right]$$

$$+ (1+\xi)^2\left[- \frac{u_1}{4} + \frac{u_2}{2} - \frac{u_3}{4} - \frac{u_5}{4} - \frac{u_6}{2} - \frac{u_7}{4}\right]. \qquad (18)$$

The derivatives $\frac{\partial v}{\partial \xi}$ and $\frac{\partial v}{\partial \eta}$ are in exactly the same form with v_i in place of u_i. Note that the first term, which is designated by (*), in equation (18) will equal zero if the following constraints are imposed,

$$u_7 = u_8 = u_1$$

and (19a,b)

$$v_7 = v_8 = v_1.$$

This is a key condition which will be used in studying the element singularity.

At any point along the line Θ = constant (η = constant), equations (17) and (18) will depend only on ξ. Therefore these equations can be rewritten as,

$$\frac{\partial u}{\partial \xi} = A_o + A_1(1+\xi),$$

(20a,b)

$$\frac{\partial u}{\partial \eta} = B_o + B_1(1+\xi)+B_2(1+\xi)^2,$$

$$\frac{\partial v}{\partial \xi} = C_o + C_1(1+\xi),$$

and (20c,d)

$$\frac{\partial v}{\partial \eta} = D_o + D_1(1+\xi) + D_2\ (1+\xi)^2$$

where A_o, A_1, B_o, B_1, B_2, C_o, C_1, D_o, D_1, D_2 are constants for any given set of nodal displacements along any line θ = constant.

Strains are equal to

$$\begin{bmatrix} \varepsilon_x \\ \varepsilon_y \\ \varepsilon_{xy} \end{bmatrix} = \begin{bmatrix} \frac{\partial u}{\partial x} \\ \frac{\partial v}{\partial y} \\ \frac{\partial u}{\partial y} + \frac{\partial v}{\partial x} \end{bmatrix} \tag{21}$$

and

$$\begin{bmatrix} \frac{\partial u}{\partial x} & \frac{\partial v}{\partial x} \\ \frac{\partial u}{\partial y} & \frac{\partial v}{\partial y} \end{bmatrix} = \begin{bmatrix} I_{11} & I_{12} \\ I_{21} & I_{22} \end{bmatrix} \begin{bmatrix} \frac{\partial u}{\partial \xi} & \frac{\partial v}{\partial \xi} \\ \frac{\partial u}{\partial \eta} & \frac{\partial v}{\partial \eta} \end{bmatrix}. \tag{22}$$

Substituting equations (12) and (19) into equation (21) and performing the operation will yield

$$\frac{\partial u}{\partial x} = \frac{A'_o}{r} + \frac{A'_1}{r} + A'_2,$$

$$\frac{\partial u}{\partial y} = \frac{B'_o}{r} + \frac{B'_1}{r} + B'_2, \tag{23a-c}$$

$$\frac{\partial v}{\partial x} = \frac{c'_o}{r} + \frac{c'_1}{r} + c'_2,$$

and

$$\frac{\partial v}{\partial y} = \frac{D'_o}{r} + \frac{D'_1}{r} + D'_2 \qquad (23d)$$

where A'_o, A'_1, A'_2, B'_o, B'_1, B'_2, C'_o, C'_1, C'_2, D'_o, D'_1, D'_2 are constants for any radial line (θ = constant), and are independent of r.

If the constraints of equations (19a) and (19b) on the nodal displacements at the crack-tip are imposed, then equations (20a) through (20d) reduce to

$$\frac{\partial u}{\partial \xi} = A_o + A_1(1+\xi),$$

$$\frac{\partial u}{\partial \eta} = B_1(1+\xi) + B_2(1+\xi)^2, \qquad (24a\text{-}d)$$

$$\frac{\partial v}{\partial \xi} = C_o + C_1(1+\xi),$$

and

$$\frac{\partial v}{\partial \eta} = D_1(1+\xi) + D_2(1+\xi)^2.$$

The derivatives will respect to x and y then reduce to

$$\frac{\partial u}{\partial x} = \frac{A'_o}{r} + A'_2,$$

$$\frac{\partial u}{\partial y} = \frac{B'_o}{r} + B'_2, \qquad (25a\text{-}c)$$

$$\frac{\partial v}{\partial x} = \frac{C'_o}{r} + C'_2,$$

and

$$\frac{\partial v}{\partial y} = \frac{D'_o}{r} + D'_2. \qquad (25d)$$

As $r \rightarrow 0$, the terms in equations (23a) through (23d) tend toward $(1/r)$ while the terms in equations (25a) through (25d) tend toward $(1/\sqrt{r})$. In both sets of equations, constant terms remain to represent the constant-strain terms associated with thermal loads. Therefore, if nodes 1, 7 and 8 at the crack-tip are restricted to having the same displacements, the elastic inverse square root singularity will occur. However, if nodes, 1, 7 and 8 are left free to displace independently of each other, the perfectly plastic inverse singularity will occur.

2.3 BOPACE

The finite element program which was used to model the edge-cracked beam in tension was BOPACE 3D (The Boeing Plastic Analysis Capability for Engines) Version 6.2. The program was originally developed by Boeing, Inc. for NASA for use in the analysis of the Space-shuttle main engines.

Many parameters which are ideal for modeling both elastic and elastic-plastic fracture problems are contained in the program. For crack problems, a convenient option available is the choice of proportionate or serendipity mapping [15]. It is through the serendipity mapping that the crack-tip elements are formed. For elastic-plastic analysis, the program employs an isotropic-kinematic hardening theory, the Huber-Mises yield surface criterion and the Prandtl-Reuss flow rule [19]. A choice of three different iterative schemes are also available for the solution of elastic-plastic problems.

CHAPTER III

ANALYSIS OF A SINGLE EDGE-CRACKED BEAM SUBJECTED TO MODE I TENSILE LOADING

3.1 Method of Approach

The analysis of the single edge-cracked beam subjected to Mode I tensile loading was completed for both the elastic and elastic-perfectly plastic cases. Two-dimensional finite element models were constructed for both cases. In the elastic case, Mode I stress intensity factors were numerically determined from crack-tip nodal displacements [Appendix A]. The Mode I stress intensity factors obtained from the finite element model nodal displacements were then compared to the Mode I stress intensity factors obtained from a boundary collocation solution [Appendix B]. Both plane stress and plane strain cases were modelled and analyzed. For the elastic-perfectly plastic cases, the size and character of the plastic zones were analyzed.

3.2 Finite Element Meshes

In the elastic models, proportionate elements (8-node quads) were used everywhere except for the few elements immediately surrounding the crack-tip where elastic crack-tip elements were employed (Figures 2 and 3). Because of symmetry, only the upper half-plane of the edge-cracked beam was modeled. Therefore, all nodes on the x-axis to the right of and including the crack-tip nodes were restrained from any displacement in the y-direction. A uniform tensile stress was applied to the top row of elements. The only difference between finite element models A and B are the number of nodes at the crack-tip and the geometry of the crack-tip elements.

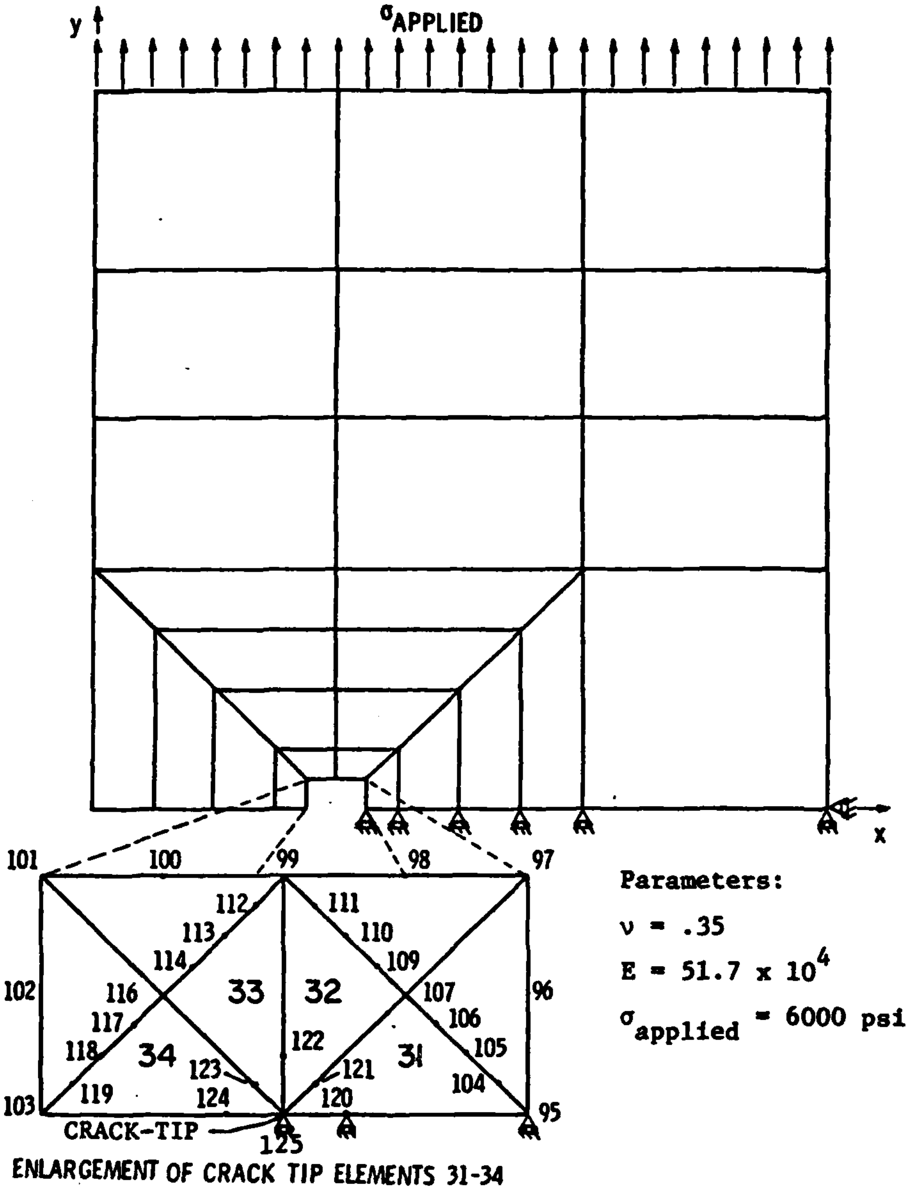

Figure 2. Elastic Finite Element Model A.

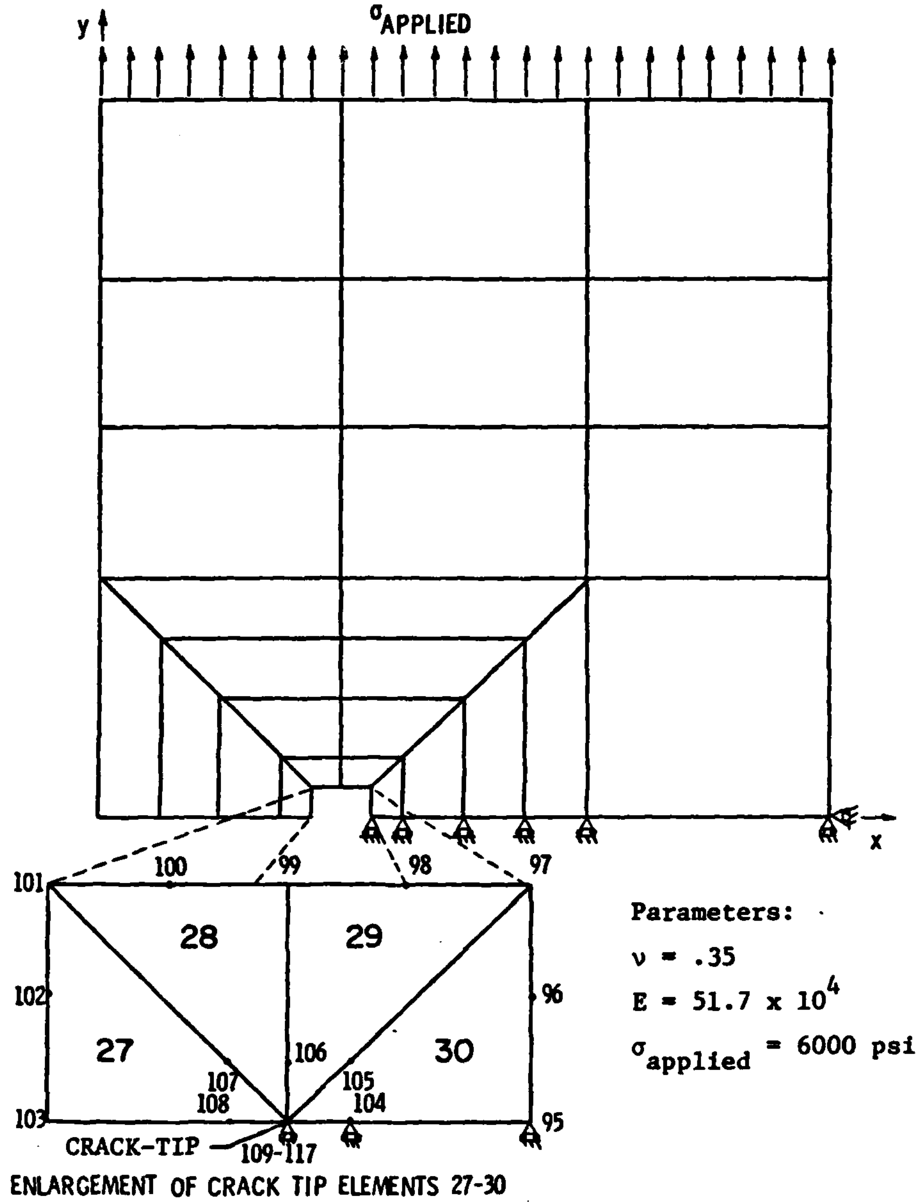

Figure 3. Elastic Finite Element Model B.

In the case of the elastic-perfectly plastic models, proportionate elements (8-node quads) were used everywhere except for the few elements immediately surrounding the crack-tip. Perfectly-plastic crack-tip elements were used to surround this area (Figures 4 and 5). Only the upper half-plane of the edge-cracked beam was modelled. Therefore, all nodes on the x-axis to the right of the crack-tip nodes were restrained from displacement in the y-direction. As in the elastic case, a uniform tensile stress was applied to the top row of elements.

3.3 Elastic Results and Discussion

The displacement results immediately surrounding the crack-tip of the elastic single edge-cracked beam subjected to Mode I tensile loading are presented in Figures 6-13. Finite element model results in terms of crack-tip nodal displacements are compared with the theoretical solutions obtained from the classic near field singularity solution [1] and appropriate stress-intensity factor. These displacement results along with additional results surrounding the crack-tip vicinity are also presented in tabular form in Appendix D.

As can be seen in the figures, the best elastic results were attained at the quarter-point nodes of finite element model B. This was the model with 9 restrained nodes at the crack-tip. The difference between these finite element model results and the theoretical solution ranged from 0-4% for both the plane stress and plane strain assumptions. Therefore, use of the finite element model displacements at the quarter-point nodes would result in Mode I stress intensity factors with comparable accuracy.

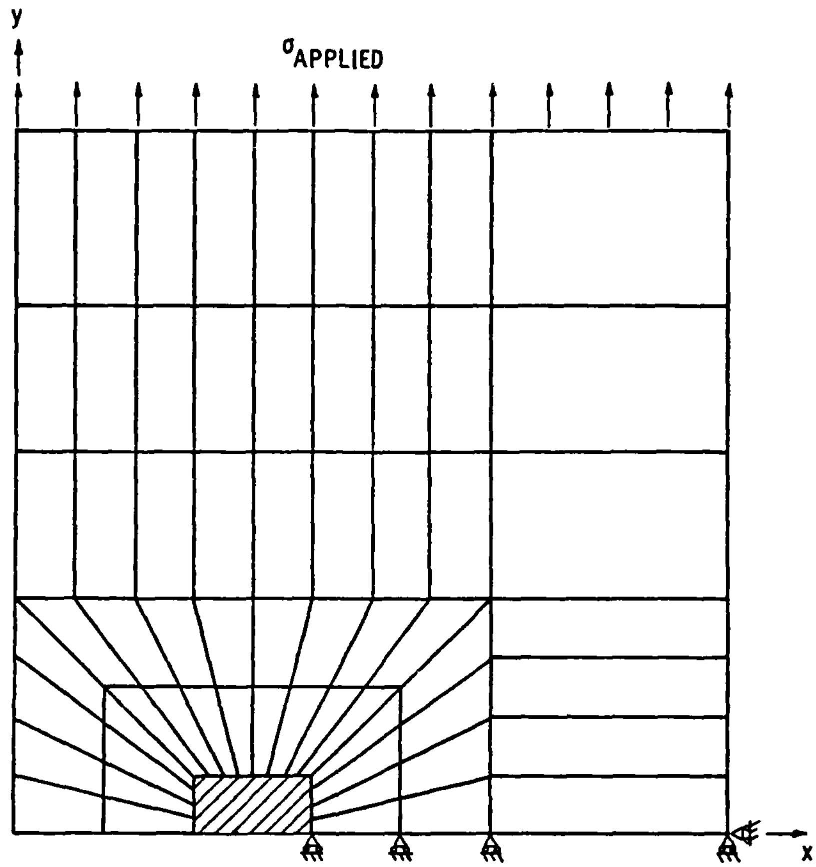

////-Crack-tip region

Parameters: $\nu = .35$

$E = 10 \times 10^6$

$\sigma_{applied} = 12,000$ psi

$\sigma_{yield} = 60,000$ psi

Figure 4. Elastic-Perfectly Plastic Finite Element Model C.

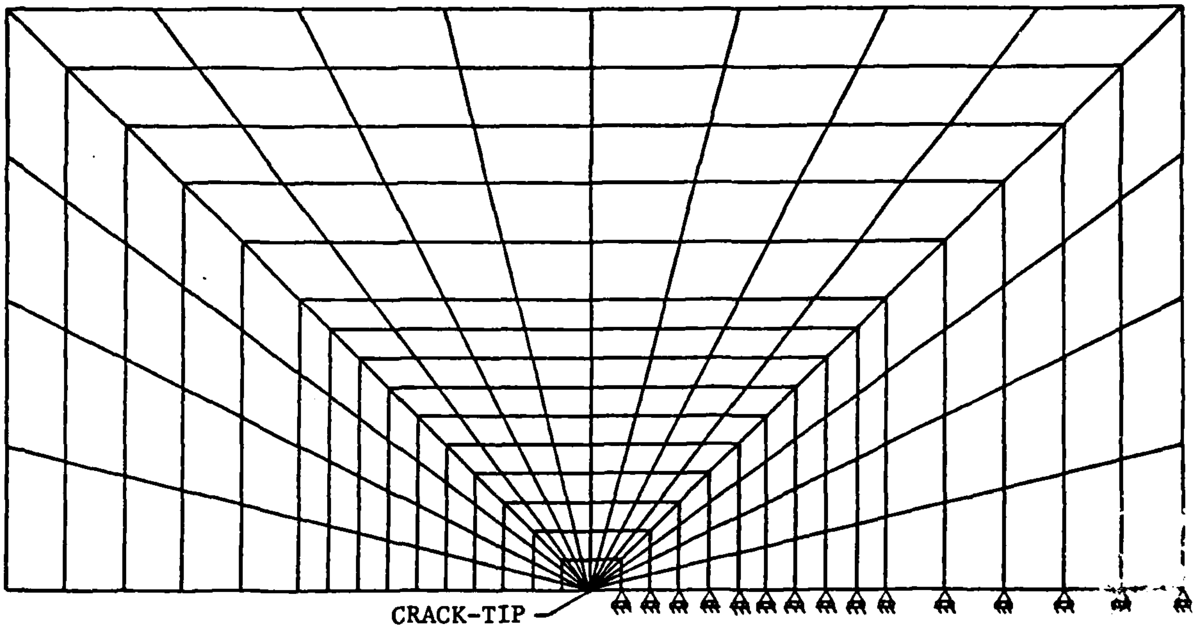

Figure 5. Magnification of Crack-tip Region in Elastic-Perfectly Plastic Finite Element Model C.

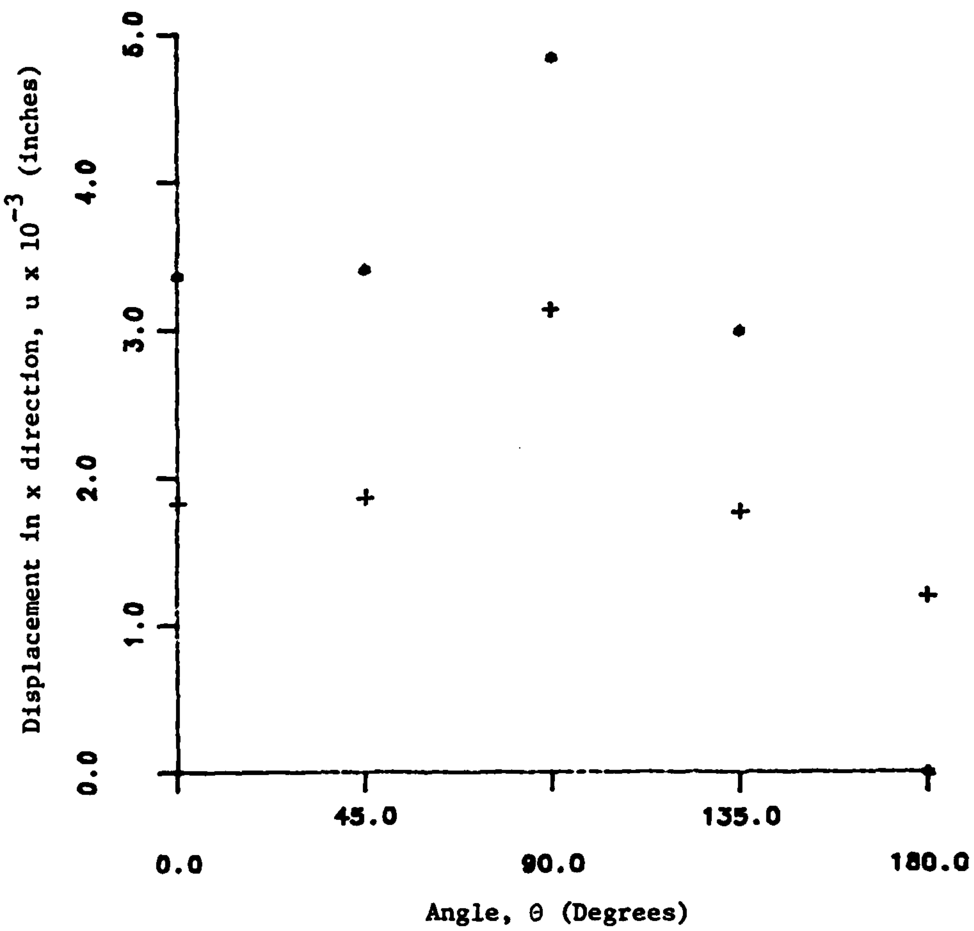

+ = Finite element model results at quarter-point nodes
* = Theoretical solution results at quarter-point nodes

Figure 6. Finite Element Model A Results (Plane Stress Assumption).

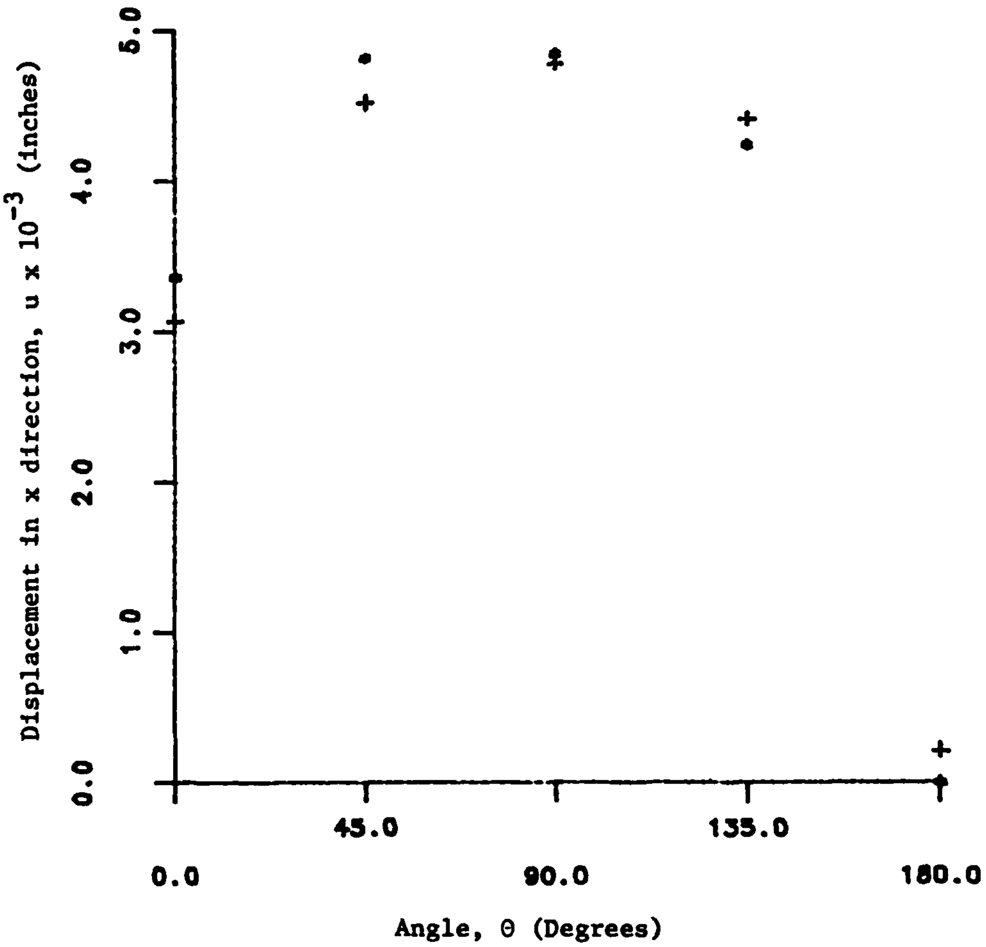

+ = Finite element model results at quarter-point nodes
* = Theoretical solution results at quarter-point nodes

Figure 7. Finite Element Model B Results (Plane Stress Assumption).

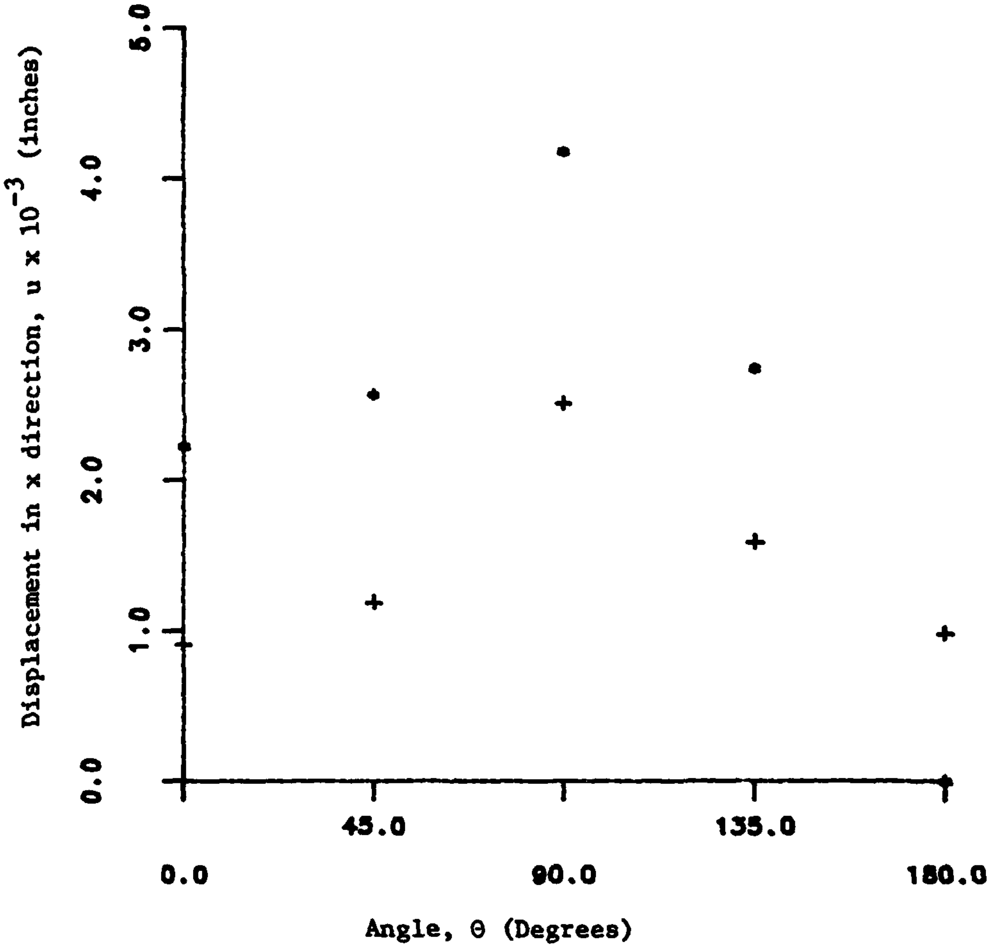

+ = Finite element model results at quarter-point nodes
* = Theoretical solution results at quarter-point nodes

Figure 8. Finite Element Model A Results (Plane Strain Assumption).

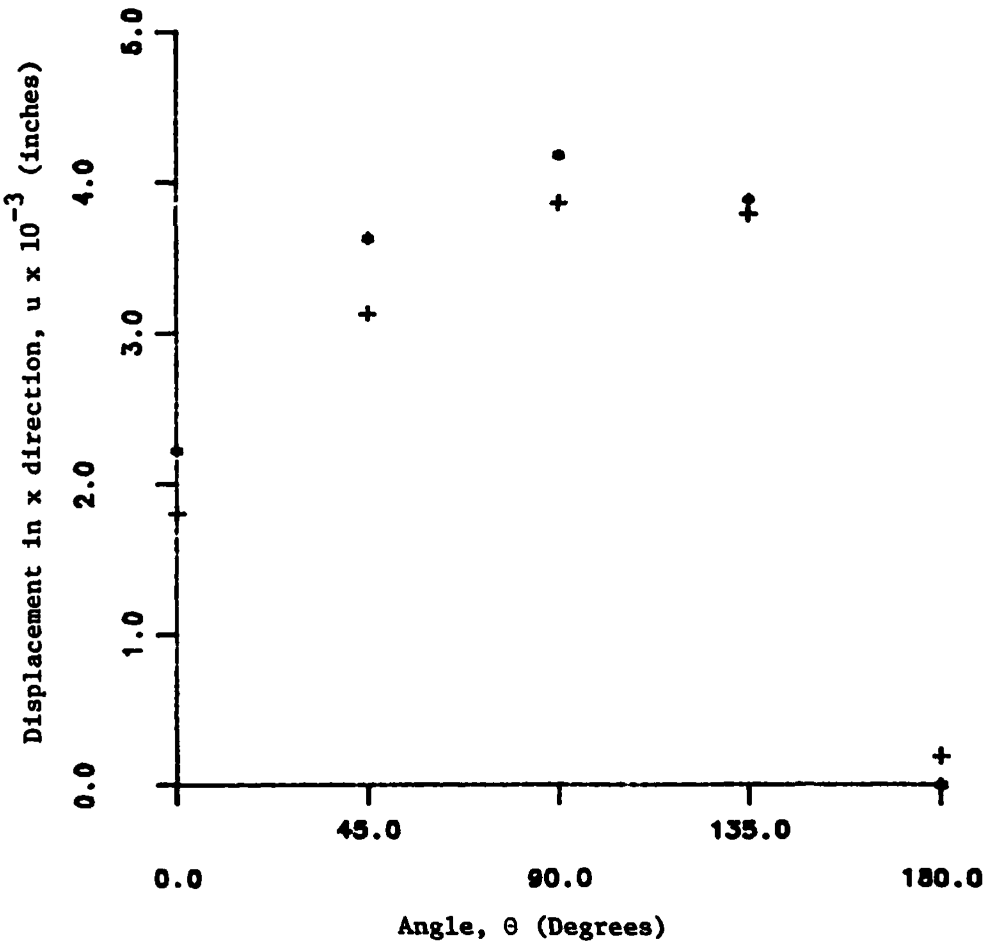

+ = Finite element model results at quarter-point nodes
* = Theoretical solution results at quarter-point nodes

Figure 9. Finite Element Model B Results (Plane Strain Assumption).

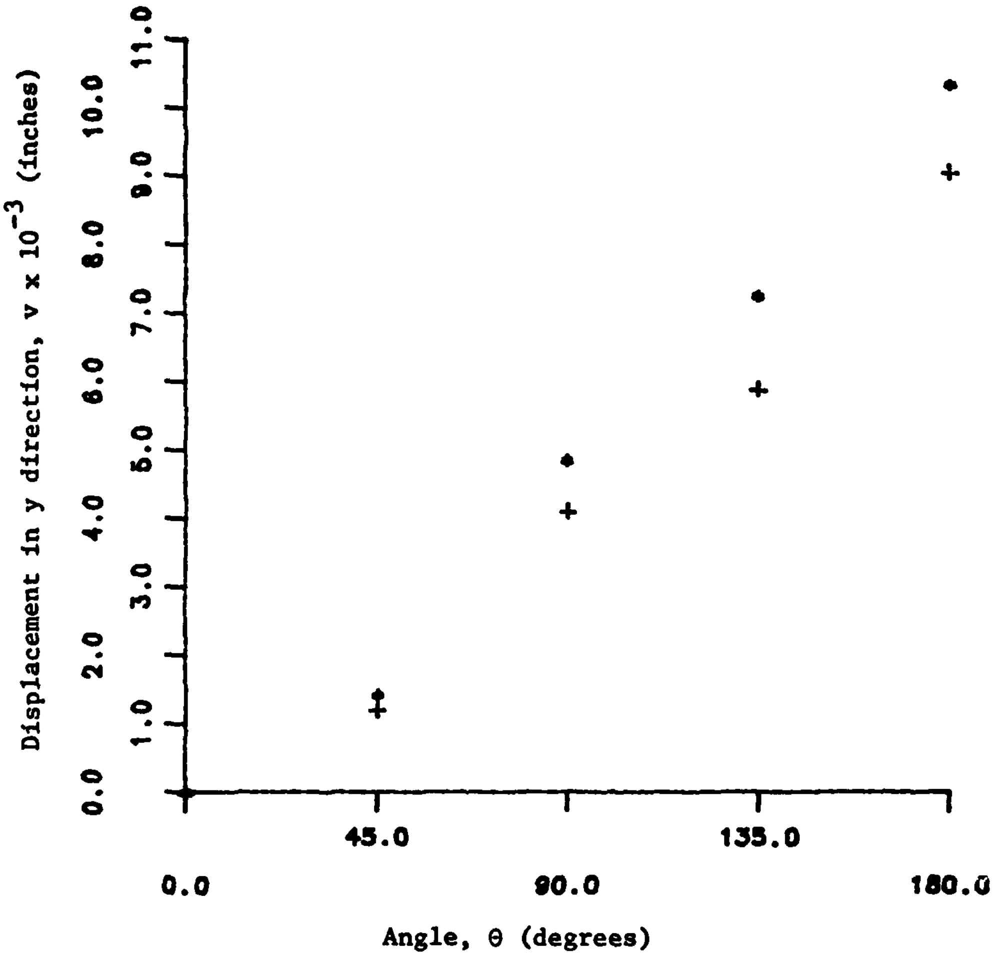

+ = Finite element model results at quarter-point nodes
* = Theoretical solution results at quarter-point nodes

Figure 10. Finite Element Model A Results (Plane Stress Assumption).

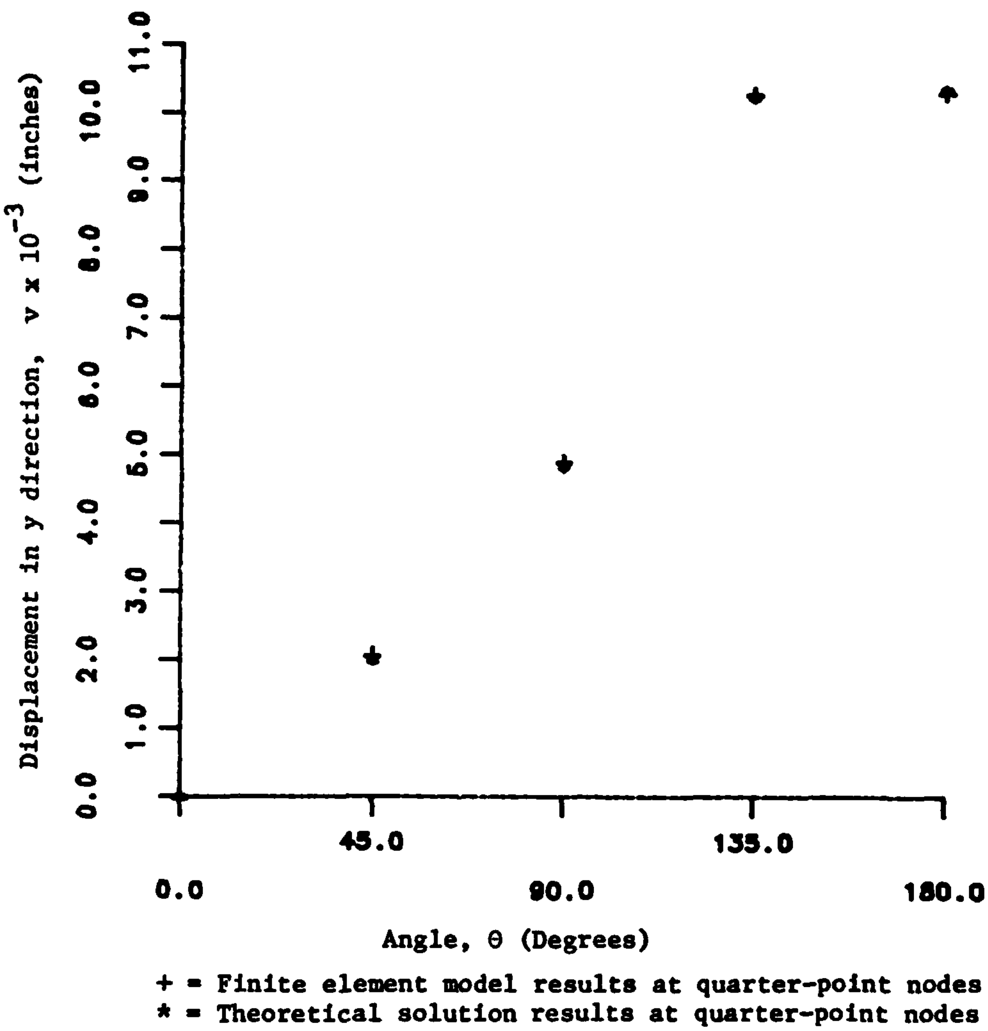

Figure 11. Finite Element Model B Results (Plane Stress Assumption).

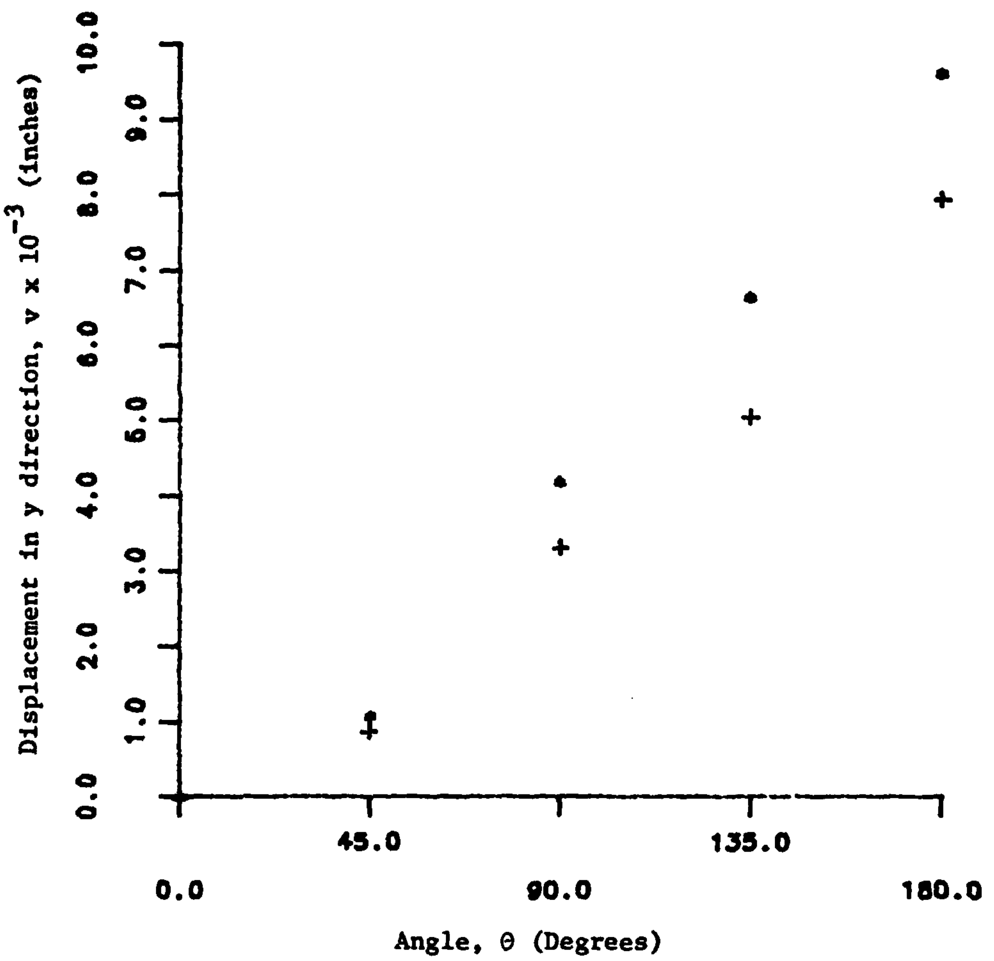

+ = Finite element model results at quarter-point nodes
* = Theoretical solution results at quarter-point nodes

Figure 12. Finite Element Model A Results (Plane Strain Assumption).

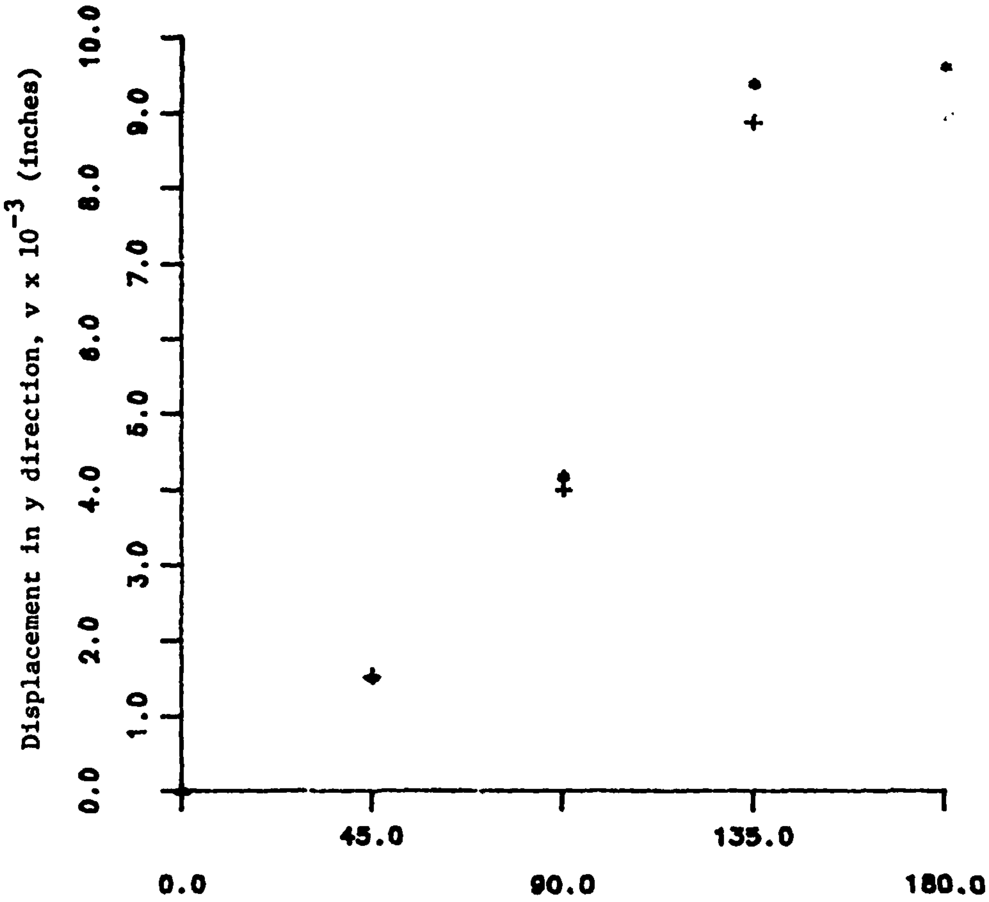

Angle, θ (Degrees)

+ = Finite element model results at quarter-point nodes
* = Theoretical solution results at quarter-point nodes

Figure 13. Finite Element Model B Results (Plane Strain Assumption).

3.4 Elastic-Perfectly Plastic Results and Discussion

Results for the elastic-perfectly plastic crack-tip analysis are shown in Figures 14-17. Results presented include examination of the extent and character of the plastic zone for both plane stress and plane strain conditions and predicted displacements along the free flank of the crack. The elastic finite element model crack flank displacements are also presented to verify that the model is behaving correctly by comparing finite element displacements to those predicted by the analytical elastic solution.

In Figure 14, plane stress was assumed for the two-dimensional finite element model and the characteristic plane stress plastic zone shape was attained [21]. Immediately outside the plastic zone, the y-displacements were examined along the crack flank to determine whether they still followed a $1/\sqrt{r}$ relationship. As is evident, the y-displacements from the elastic-perfectly plastic finite element model were greater in magnitude than both the predicted elastic values and the elastic finite element values. Not only were the y-displacements greater in magnitude, but they did not follow the $1/\sqrt{r}$ relationship characteristic of the elastic displacements. This can be explained by the increased compliance due to the plastic zone. Another approach was therefore attempted. In this approach, the concept of an equivalent crack length was introduced. In order to predict the elastic-perfectly plastic results, the same linear elastic Mode I displacement equations are used with the plastic zone being treated as nothing more than an extension to the crack length, r_y. The origin of the axis system, however, is still located at the original crack-tip. A similar approach was adopted in the past by F. A. McClintock

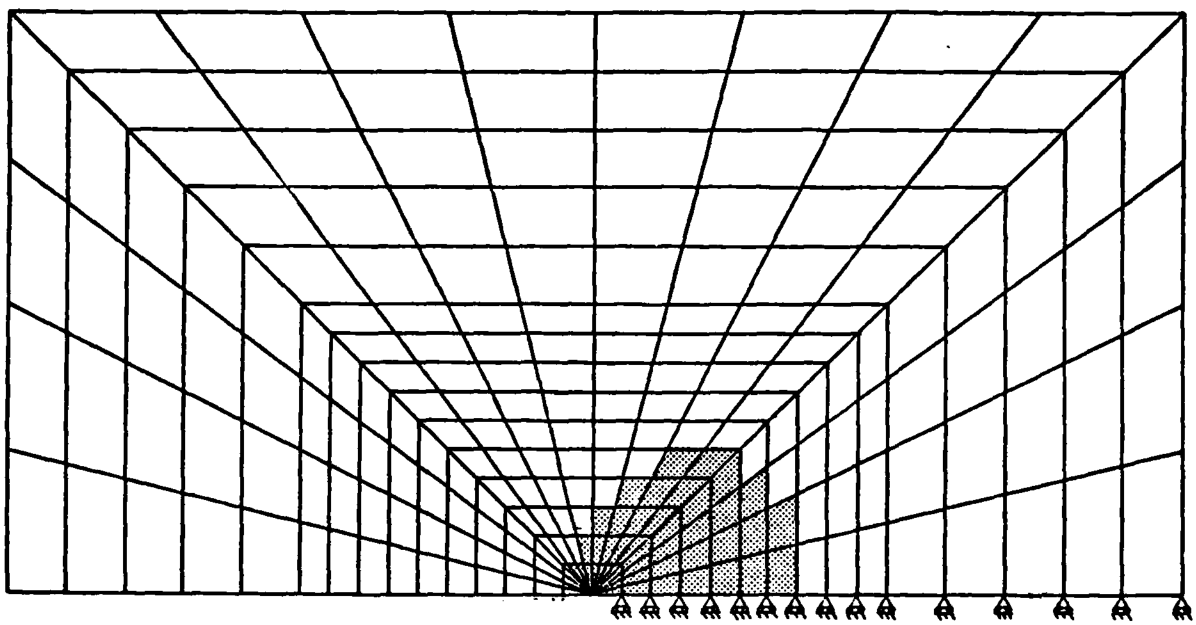

Figure 14. Plane Stress Plastic Zone Observed in Elastic-Perfectly Plastic Finite Element Model C.

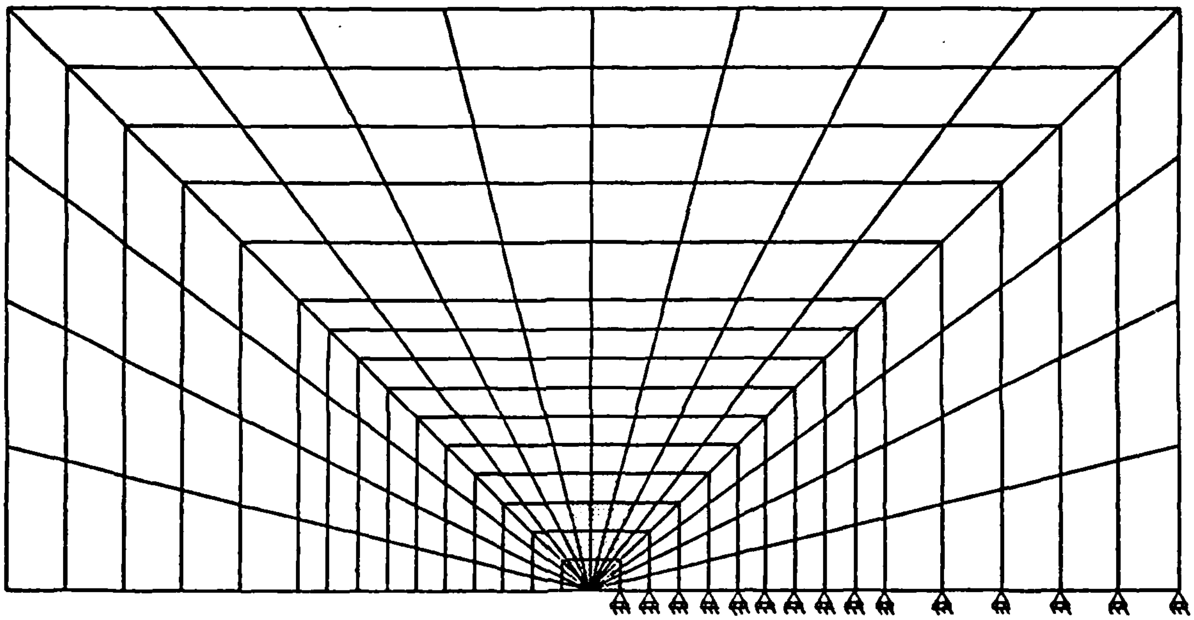

Figure 15. Plane Strain Plastic Zone Observed in Elastic-Perfectly Plastic Finite Element Model C.

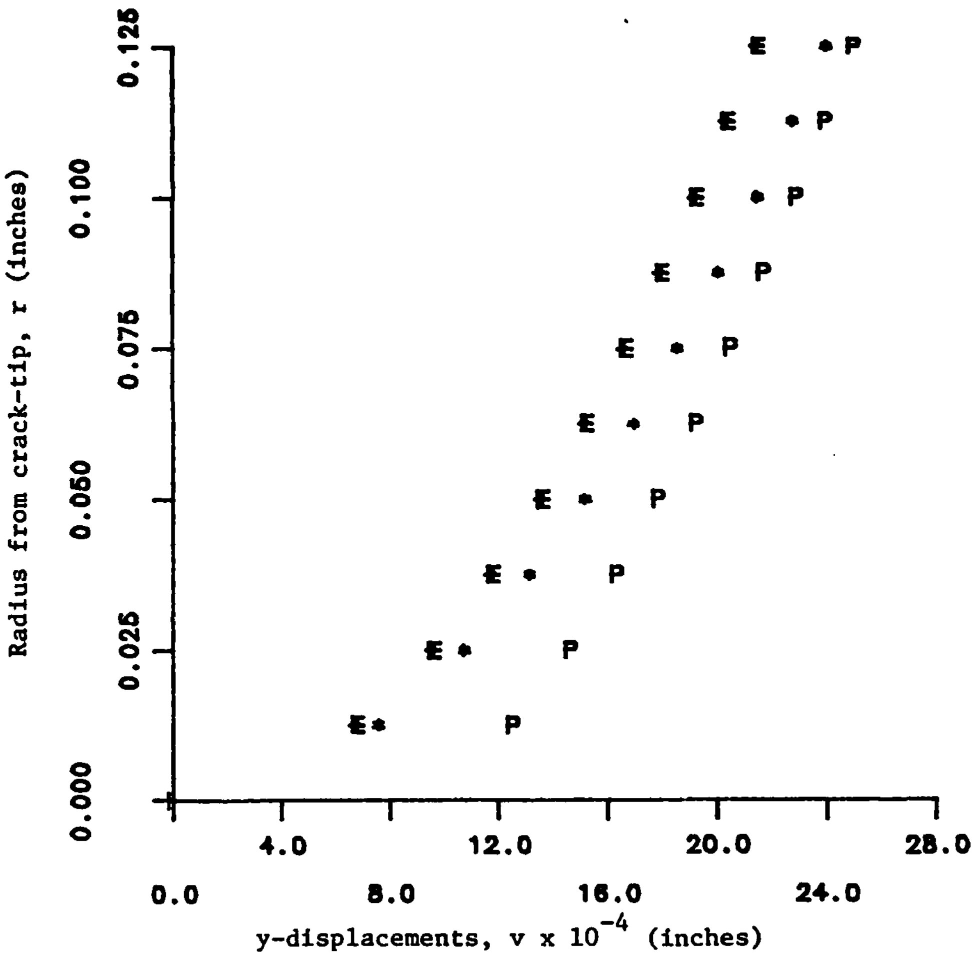

E = Elastic finite element model results along crack flank
P = Elastic-perfectly plastic finite element model results along crack flank
+ = Predicted elastic y-displacement along crack flank
* = Predicted y-displacements along crack flank using the equivalent crack length

Figure 16. Elastic/plastic Results (Plane Stress Assumption).

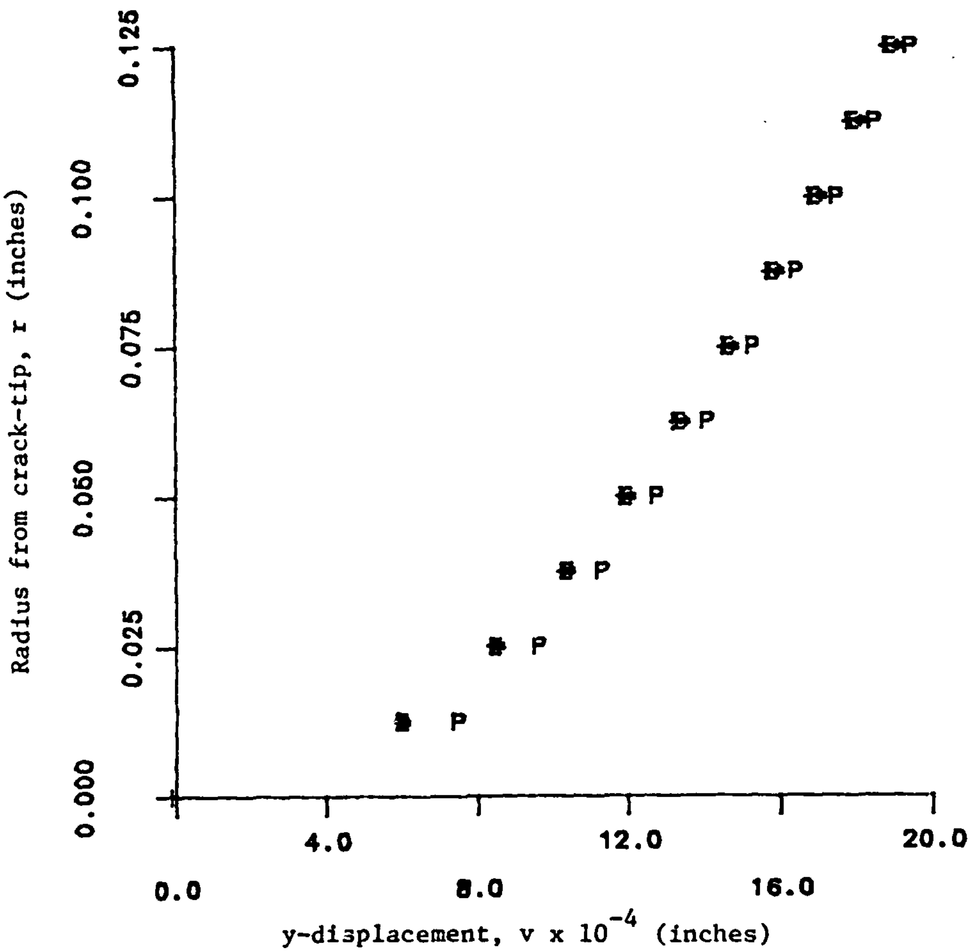

E = Elastic finite element model results along crack flank
P = Elastic-perfectly plastic finite element model results along crack flank
+ = Predicted elastic y-displacements along crack flank
* = Predicted y-displacements along crack flank using the equivalent crack length

Figure 17. Elastic/Plastic Results (Plane Strain Assumption).

and G. R. Irwin in an analysis for the Mode III case [22]. Figure 16 shows the results from this approach. Again, the predicted y-displacements attained by using the equivalent crack length did not fit the elastic-perfectly plastic finite element model results but did approach them asymptotically with increasing distance from the crack-tip.

In Figure 15, plane strain was assumed for the two-dimensional finite element model and the characteristic plane strain plastic zone was attained [21]. Again as in the plane stress model, the y-displacements along the crack flank outside the plastic zone were examined to see if they followed a $1/\sqrt{r}$ relationship. However, the y-displacements from the elastic-perfectly plastic finite element model were greater in magnitude than the predicted elastic values and did not show the $1/\sqrt{r}$ relationship (Figure 17). As in the plane stress case, the equivalent crack length approach was again used to predict the plane strain elastic-perfectly plastic results. These results are presented in Figure 17. Again the predicted y-displacements attained by using the equivalent crack length did not fit the elastic-perfectly plastic finite element model results but did approach them asymptotically with increasing distance from the crack-tip.

CHAPTER IV

SUMMARY AND CONCLUSIONS

By constructing various two-dimensional finite element models for a single edge-cracked beam subjected to Mode I tensile loading, a thorough analysis of the stresses, strains and displacements surrounding the crack-tip was performed. Particular emphasis was placed on 1) determining the Mode I stress intensity factor in the elastic models via a displacement method and 2) examining the size and character of the plastic zone in the elastic-perfectly plastic models. In all of the finite element models, either special elastic or plastic crack-tip elements were used to create the crack-tip singularity.

The elastic finite element model results do indeed represent accurate crack-tip singularity effects as was made evident by a comparison with available analytical solutions. Not only do the elastic models represent the singularity effect accurately, but with the aid of the special elastic crack-tip elements, they are able to do it with a minimal amount of elements. This leads to a significant savings in both time and costs

The elastic-perfectly plastic finite element model results were also of great interest. The plastic zones obtained from the finite element models did indeed agree with the characteristic plane stress and plane strain plastic zones. However, the equivalent crack length approach did not yield accurate results for the y-displacements along the crack flank for either the plane strain or plane stress case.

CHAPTER V

RECOMMENDATIONS FOR FUTURE RESEARCH

A great deal of additional research can and should be conducted in applying the finite element method to fracture mechanics problems. With the improved finite element programs available, several promising areas can be investigated.

One area which can be pursued further is the investigation of a three-dimensional elastic finite element model for a single edge-cracked beam subjected to Mode I tensile loading. With a three-dimensional model, one could determine the effect of model thickness on stress state (plane stress or plane strain) at the crack-tip. Finite element model results could then be compared to empirical and experimental results. One experimental technique which has been used to investigate this area is scattered-light photo-elasticity [20].

Another area which should be pursued is the investigation of a three-dimensional elastic-perfectly plastic finite element model for a single edge-cracked beam subjected to Mode I tensile loading. With a three-dimensional elastic-perfectly plastic finite element model a three-dimensional characterization of the plastic zone surrounding the crack-tip line could be attained.

Finally a thorough investigation of the J-integral as it is applied in the area of elastic/plastic fracture mechanics should be considered.

In any investigation, a careful, well drawn out in advance, stepwise procedure from the simple to the more complex case should

be undertaken. It is this type of procedure which allows one to gain valuable experience with the actual "inner workings" of every aspect of the computer model and will assure one of accurate results. Therefore, in the investigation of three-dimensional finite element models, simple models with coarse-grids should be constructed first. These models should then be thoroughly analyzed to verify that everything is operating correctly. If any problems do occur, they are easily seen and can be corrected. Once everything has been checked and is operating correctly in the simple, coarse-grid models, larger and/or finer-grid models may be generated.

BIBLIOGRAPHY

1. Paris, P. C. and Sih, G. C., "Stress Analysis of Cracks," ASTM, STP, No. 381, pp. 30-81.

2. Tracy, D. M., "Finite Elements for Three-Dimensional Elastic Crack Analysis," Nuclear Engineering and Design, V. 26 (1974), pp. 282-290.

3. Miller, K. J. and Kfouri, A. P., "An Elastic-plastic Finite Element Analysis of Crack-Tip Fields Under Biaxial Loading Conditions," International Journal of Fracture, V. 10, No. 3 (September 1974), pp. 393-403.

4. Henshell, R. D. and Shaw, K. G., "Crack-Tip Finite Elements are Unnecessary," International Journal of Numerical Methods in Engineering, V. 9, (1975), pp. 495-507.

5. Barsoum, R. S., "On the Use of Isoparametric Finite Elements in Linear Fracture Mechanics," International Journal of Numerical Methods in Engineering, V. 10 (1976), pp. 25-37.

6. Barsoum, R. S., "Triangular Quarter-Point Elements as Elastic and Perfectly Plastic Crack-Tip Elements," International Journal of Numerical Methods in Engineering, V. 11 (1977), pp. 85-98.

7. Pu, S. L., Hussain, M. A. and Lorensen, W. E., "The Collapsed Cubic Isoparametric Element as a Singular Element for Crack Problems," International Journal of Numerical Methods in Engineering, V. 12, (1978), pp. 1727-1742.

8. Wilson, W. K., "A Comparison of Finite Element Solutions for an Elastic-plastic Crack Problem," International Journal of Fracture, V. 14, (1978), pp. R95-R108.

9. Faukes, A. J., "An Assessment of Crack-Tip Singularity Models for Use With Isoparametric Elements," Engineering Fracture Mechanics, V. 11 (1979), pp. 143-159.

10. Steinmueller, G., "Restrictions in the Application of Automatic Mesh Generation Schemes by Isoparametric Coordinates," International Journal for Numerical Methods in Engineering, V. 8, (1974), pp. 289-294.

11. Chan, S. K., Tuba, I. S. and Wilson, W. K., "On the Finite Element Method in Linear Fracture Mechanics," Engineering Fracture Mechanics, V. 2, (1970), pp. 1-17.

12. Hoyniak, D. and Conway, J. C., "Finite Element Analysis of the Compact Shear Specimen," Engineering Fracture Mechanics, V. 12, (1979), pp. 301-306.

13. Conway, J. C., "Finite Element Techniques Applied to Cracks Interacting With Selected Singularities," Journal of the American Ceramic Society, V. 58, No. 9-10, (September-October 1975), pp. 402-405.

14. Tada, H., Paris, P. C., and Irwin, G. R., The Stress Analysis of Cracks Handbook, Del Research Corporation, Hellertown, Pennsylvania, (1973), pp. 2-24.

15. Zienkiewicz, O. C., The Finite Element Method, Third Edition, McGraw-Hill, (1977).

16. Gross, B. and Srawley, J. E., "Stress Intensity Factors for a Single Edge Notch Tension Specimen by Boundary Collocation of a Stress Function," NASA TN D-2395, (1964).

17. Brown, W. F. and Srawley, J. E., "Plane Strain Crack Toughness Testing of High Strength Metallic Materials," ASTM Special Technical Publication, No. 410, (1966).

18. Proger, W., "The Theory of Plasticity: A Survey of Recent Achievements," Proceedings of the Institution for Mechanical Engineering, V. 169, (1955).

19. Johnson, W. and Mellor, P. B., "Engineering Plasticity," Van Nostrand Reinhold (1978).

20. Ross, E., Kaminski, G. and Conway, J. C., "Measurement of Mode I Stress-intensity Factors by Scattered-light Photoelasticity," Experimental Mechanics, March (1982), pp. 117-120.

21. Barsom, J. and Rolfe, S., "Fracture and Fatigue Control in Structures," Prentice-Hall, Inc. (1977), p. 60.

22. McClintock, F. A. and Irwin, G. R., "Plasticity Aspects of Fracture Mechanics," ASTM, STP No. 381, pp. 84-113.

23. Eftis, J., Subramonian, N. and Liebowitz, H., "Crack Border Stress and Displacement Equations Revisited," Engineering Fracture Mechanics, V. 9 (1977), pp. 189-210.

APPENDIX A

ELASTIC CRACK-TIP STRESS AND DISPLACEMENT FIELDS

Refering to Figure A1, the well-known Mode I stress and displacement fields surrounding a crack-tip [1, 23] are given by

$$\sigma_x = \frac{K_I}{\sqrt{2\pi r}} \cos\frac{\theta}{2} \left(1 - \sin\frac{\theta}{2}\sin\frac{3\theta}{2}\right) , \qquad \text{(A-1)}$$

$$\sigma_y = \frac{K_I}{\sqrt{2\pi r}} \cos\frac{\theta}{2} \left(1 + \sin\frac{\theta}{2}\sin\frac{3\theta}{2}\right) , \qquad \text{(A-2)}$$

$$\tau_{xy} = \frac{K_I}{\sqrt{2\pi r}} \sin\frac{\theta}{2} \cos\frac{\theta}{2} \cos\frac{3\theta}{2}, \qquad \text{(A-3)}$$

$$\sigma_z = \nu(\sigma_x + \sigma_y) \text{ for the plane strain assumption,} \qquad \text{(A-4)}$$

$$\sigma_z = 0 \text{ for the plane stress assumption,} \qquad \text{(A-5)}$$

$$u = \frac{K_I}{G} \left(\frac{r}{2\pi}\right)^{\frac{1}{2}} \cos\frac{\theta}{2} \left[\frac{1}{2}(F-1) + \sin^2\frac{\theta}{2}\right], \qquad \text{(A-6)}$$

$$v = \frac{K_I}{G} \left(\frac{r}{2\pi}\right)^{\frac{1}{2}} \sin\frac{\theta}{2} \left[\frac{1}{2}(F+1) - \cos^2\frac{\theta}{2}\right], \qquad \text{(A-7)}$$

where $F = \frac{3-\nu}{1+\nu}$ for the plane stress assumption,

and $F = 3-4\nu$ for the plane strain assumption.

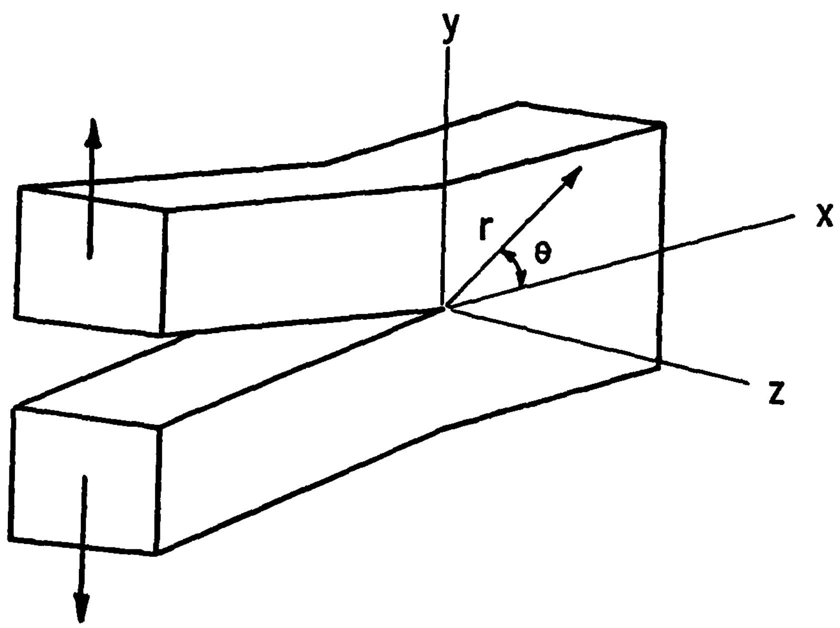

Figure A1. Mode I Loading.

APPENDIX B

SINGLE EDGE NOTCH TEST SPECIMEN

From reference 14 the Mode I stress intensity factor for the single edge-cracked plate (Figure B1) is given as:

$$K_I = \sigma \sqrt{\pi a} \; F(a/b).$$

Empirical formulas for F(a/b) are given as:

1. $$F(a/b) = 1.12 - .231\ (a/b) + 10.55\ (a/b)^2 - 21.72\ (a/b)^3 + 30.39\ (a/b)^4 \qquad \text{(B-1)}$$

   Gross 1964, Brown 1966; Boundary Collocation Method

   Accuracy: .5% for $a/b \leq .6$

2. $$F(a/b) = .265\ (1-a/b)^4 + \frac{.857 + .265\ (a/b)}{(1-a/b)^{3/2}} \qquad \text{(B-2)}$$

   Tada 1973

   Accuracy: 1% for $a/b < .2$; .5% for $a/b \geq .2$

3. $$F(a/b) = \sqrt{\frac{2b}{\pi a} \tan \frac{\pi a}{2b}} \; \frac{.752 + 2.02\ (a/b) + .37\left(1 - \sin \frac{\pi a}{2b}\right)^2}{\cos \frac{\pi a}{2b}} \qquad \text{(B-3)}$$

   Tada 1973

   Accuracy: .5% for any a/b

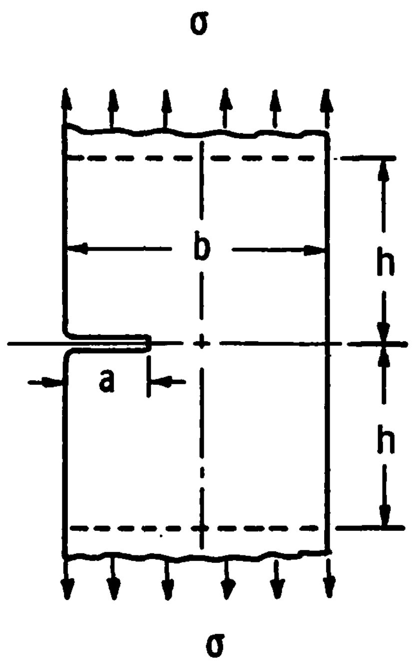

Figure B1. Edge Notch Speciman.

APPENDIX C

STRAIN ENERGY RELATIONS

From strain energy relations the strain energy release rate is given as

$$G_I = \frac{K_I^{\,2}}{E} \quad \text{for plane stress,} \tag{C-1}$$

and

$$G_I = \frac{1-\nu^2}{E} K_I^{\,2} \quad \text{for plane strain.} \tag{C-2}$$

Rearranging equations (C-1) and (C-2) yields

$$K_I = \sqrt{EG_I} \quad \text{for plane stress} \tag{C-3}$$

and

$$K_I = \sqrt{\frac{EG_I}{(1-\nu^2)}} \quad \text{for plane strain.} \tag{C-4}$$

Therefore

$$(K_I)_{\text{PLANE STRAIN}} = 1.06\,(K_I)_{\text{PLANE STRESS}}. \tag{C-5}$$

APPENDIX D

ELASTIC FINITE ELEMENT MODEL RESULTS

Table D-1. Model A Displacement Results (Plane Stress Assumption).

θ (degrees)	r (inches)	Node	Theoretical x-displacement, $u \times 10^{-3}$ in.	FEM x-displacement, $u \times 10^{-3}$ in.	Theoretical y-displacement, $v \times 10^{-3}$ in.	FEM y-displacement, $v \times 10^{-3}$ in.
180^o	.03125	124	0	-1.97	10.335	9.045
135^o	.0221	123	2.997	1.766	7.236	5.880
90^o	.03125	122	4.841	3.136	4.841	4.103
45^o	.0221	121	3.403	1.862	1.409	1.199
0^o	.03125	120	3.359	1.830	0	0
180^o	.125	103	0	.718	20.672	20.437
135^o	.0884	116	5.994	4.872	14.472	14.244
90^o	.125	99	9.683	8.202	9.682	9.641
45^o	.0884	107	6.806	4.868	2.819	2.945
0^o	.125	95	6.719	4.335	0	0
180^o	.1875	94	0	-2.82	25.318	24.867
135^o	.2652	93	10.383	10.195	25.066	24.961
90^o	.1875	92	11.859	10.335	11.859	11.969
45^o	.2652	91	11.789	8.846	4.883	5.249
0^o	.1875	90	8.229	5.281	0	0
180^o	.25	89	0	.126	29.234	28.728
135^o	.3536	87	11.989	12.303	28.945	28.959
90^o	.25	85	13.693	12.244	13.693	13.984
45^o	.3536	83	13.613	10.251	5.639	6.177
0^o	.25	81	9.503	6.032	0	0

Table D-2. Model A Displacement Results (Plane Strain Assumption).

Θ (degrees)	r (inches)	Node	Theoretical x-displacement, $u \times 10^{-3}$ in.	FEM x-displacement, $u \times 10^{-3}$ in.	Theoretical y-displacement, $v \times 10^{-3}$ in.	FEM y-displacement, $v \times 10^{-3}$ in.
180^o	.03125	124	0	-.978	9.613	7.932
135^o	.0221	123	2.745	1.588	6.627	5.041
90^o	.03125	122	4.183	2.513	4.183	3.302
45^o	.0221	121	2.565	1.185	1.062	.872
0^o	.03125	120	2.218	.908	0	0
180^o	.125	103	0	.432	19.226	17.910
135^o	.0884	116	5.491	4.307	13.255	12.333
90^o	.125	99	8.366	6.698	8.366	7.932
45^o	.0884	107	5.130	3.204	2.125	2.796
0^o	.125	95	4.437	2.163	0	0
180^o	.1875	94	0	-.081	23.547	21.773
135^o	.2652	93	9.509	8.930	22.959	21.699
90^o	.1875	92	10.247	8.436	10.247	9.938
45^o	.2652	91	8.885	5.899	3.680	4.034
0^o	.1875	90	5.434	2.619	0	0
180^o	.25	89	0	.265	27.189	25.151
135^o	.3536	87	10.981	10.767	26.510	25.205
90^o	.25	85	11.832	10.002	11.832	11.667
45^o	.3536	83	10.260	6.832	4.249	4.809
0^o	.25	81	.275	2.956	0	0

Table D-3. Model B Displacement Results (Plane Stress Assumption).

θ (degrees)	r (inches)	Node	Theoretical x-displacement, $u \times 10^{-3}$ in.	FEM x-displacement, $u \times 10^{-3}$ in.	Theoretical y-displacement, $v \times 10^{-3}$ in.	FEM y-displacement, $v \times 10^{-3}$ in.
180^o	.03125	108	0	.214	10.335	10.287
135^o	.0442	107	4.238	4.409	10.233	10.262
90^o	.03125	106	4.841	4.778	4.841	4.899
45^o	.0442	105	4.813	4.513	1.994	2.069
0^o	.03125	104	3.359	3.069	0	0
180^o	.125	103	0	.826	20.672	20.568
135^o	.1768	101	8.477	9.279	20.466	20.645
90^o	.125	99	9.683	9.619	9.682	9.948
45^o	.1768	97	9.626	8.628	3.987	4.299
0^o	.125	95	6.719	5.676	0	0
180^o	.1875	94	0	1.218	25.318	25.173
135^o	.2652	93	10.382	11.678	25.066	25.357
90^o	.1875	92	11.859	11.841	11.859	12.256
45^o	.2652	91	11.789	10.362	4.883	5.343
0^o	.1875	90	8.229	6.686	0	0
180^o	.25	89	0	1.588	29.234	29.086
135^o	.3536	87	11.989	13.790	28.945	29.334
90^o	.25	85	13.693	13.785	13.693	14.256
45^o	.3536	83	13.613	11.786	5.639	6.269
0^o	.25	81	9.503	7.466	0	0

Table D-4. Model B Displacement Results (Plane Strain Assumption).

Θ (degrees)	r (inches)	Node	Theoretical x-displacement, $u \times 10^{-3}$ in.	FEM x-displacement, $u \times 10^{-3}$ in.	Theoretical y-displacement, $v \times 10^{-3}$ in.	FEM y-displacement, $v \times 10^{-3}$ in.
180^o	.03125	108	0	.189	9.613	8.995
135^o	.0442	107	3.882	3.765	9.373	8.868
90^o	.03125	106	4.183	3.867	4.183	4.013
45^o	.0442	105	3.627	3.130	1.502	1.523
0^o	.03125	104	2.218	1.807	0	0
180^o	.125	103	0	.721	19.226	17.990
135^o	.1768	101	7.764	7.981	18.746	17.909
90^o	.125	99	8.366	7.793	8.366	8.230
45^o	.1768	97	7.255	5.920	3.005	3.266
0^o	.125	95	4.437	3.211		0
180^o	.1875	94	0	1.065	23.547	22.023
135^o	.2652	93	9.509	10.064	22.959	22.032
90^o	.1875	92	10.247	9.604	10.247	10.183
45^o	.2652	91	8.885	7.076	3.680	4.113
0^o	.1875	90	5.434	3.704	0	0
180^o	.25	89	0	1.386	27.189	25.449
135^o	.3536	87	10.981	11.903	26.510	25.520
90^o	.25	85	11.832	11.197	11.832	11.890
45^o	.3536	83	10.260	8.020	4.249	4.885
0^o	.25	81	6.275	4.057	0	0

DISTRIBUTION LIST FOR TM 82-131

Commander (NSEA 0342) Naval Sea Systems Command Department of the Navy Washington, DC 20362	Copies 1 and 2
Commander (NSEA 9961) Naval Sea Systems Command Department of the Navy Washington, DC 20362	Copies 3 and 4
Defense Technical Information Center 5010 Duke Street Cameron Station Alexandria, VA 22314	Copies 5 through 10

DATE
ILME
-8